Tao et al. *Zool. Res.* 2025, 46(4): 841−850
https://doi.org/10.24272/j.issn.2095-8137.2025.016
https://cstr.cn/32248.14.zr.2025.016

ZR | Zoological Research

Article Open Access

Lycium barbarum glycopeptide ameliorates aberrant neuronal activity via ER stress modulation in ventral forebrain organoids derived from depressive patients

Meng-Dan Tao[1,2,#], Can Wang[1,2,#], Xin-Hao Wu[3], Qi Chen[1], Wei-Wei Gao[1], Min Xu[1], Yuan Hong[1], Xiao Han[1,2], Wan-Ying Zhu[1], Qian Zhu[1], Yan Liu[1,2,*], Xing Guo[2,3,4,*]

[1] *Institute for Stem Cell and Neural Regeneration*, *School of Pharmacy*, *Nanjing Medical University*, *Nanjing*, *Jiangsu* 211166, *China*
[2] *State Key Laboratory of Reproductive Medicine*; *Nanjing Medical University*, *Nanjing*, *Jiangsu* 211166, *China*
[3] *Department of Neurobiology*, *School of Basic Medical Sciences*; *Nanjing Medical University*, *Nanjing*, *Jiangsu* 211166, *China*
[4] *Second Affiliated Hospital of Nanjing Medical University*, *Nanjing*, *Jiangsu* 210011, *China*

ABSTRACT

Major depressive disorder (MDD) is a debilitating psychiatric condition associated with substantial personal, societal, and economic costs. Despite considerable advances in research, most conventional antidepressant therapies fail to achieve adequate response in a significant proportion of patients, underscoring the need for novel, mechanism-based interventions. *Lycium barbarum* glycopeptide (LbGp), a bioactive compound with emerging neuroprotective properties, has been proposed as a candidate for antidepressant development; however, its therapeutic efficacy and underlying mechanisms remain largely uncharacterized. In this study, ventral forebrain organoids were generated from patients with MDD to investigate disease-related neurophysiological abnormalities. These organoids exhibited disrupted neuronal morphology, diminished calcium signaling, and impaired electrophysiological activity. Administration of LbGp effectively restored structural and functional deficits in MDD-derived organoids. Transcriptomic profiling revealed that LbGp ameliorated endoplasmic reticulum (ER) stress responses. To investigate the causative role of ER stress, control organoids were treated with the ER stress agonist CCT020312, which elicited neural activity impairments resembling those observed in MDD organoids. Notably, LbGp reversed the phenotypic consequences of CCT020312 exposure in control organoids. In conclusion, ventral forebrain organoids derived from individuals with MDD demonstrated that LbGp ameliorates disease-associated phenotypes by modulating ER stress.

Keywords: Disease modeling; GABAergic interneuron; iPSCs; Major depressive disorder; Organoids

INTRODUCTION

Depression represents one of the most prevalent and debilitating psychiatric disorders, characterized by a range of clinical symptoms including impaired sociability, anhedonia, and behavioral despair (Anderson et al., 2024; Rakel, 1999). According to the World Health Organization (WHO), major depressive disorder (MDD), including dysthymia, affects approximately 322 million individuals globally, reflecting an increase of over 18% since 2005 and establishing MDD as the leading cause of global disease burden and disability (Zimath et al., 2021). Despite significant advances in our understanding of its etiology, current pharmacological therapies are often ineffective, poorly tolerated, and associated with substantial side effects (Cuijpers et al., 2016; Yeung et al., 2018). These limitations have spurred growing interest in plant-derived compounds with neuroactive potential as alternative therapeutic strategies (Dietz et al., 2016; Janda et al., 2020). However, reliable preclinical platforms for evaluating the therapeutic efficacy and mechanisms of action in human-relevant MDD models remain underdeveloped.

Lycium barbarum (commonly known as goji berry) has been used in traditional Chinese medicine for centuries, with *Lycium barbarum* polysaccharide (LBP) identified as one of its principal active components (Dai et al., 2023; Fu et al., 2021).

Received: 25 February 2025; Accepted: 06 May 2025; Online: 07 May 2025
Foundation items: This work was supported by the National Key Research and Development Program of China (2021YFA1101800, 2022YFA1104800, 2023YFF1203600), National Natural Science Foundation of China (82325015, 82171528, U23A20429, 82371260, 21904069, 22274079, 82401794), Jiangsu Provincial Natural Science Fund for Excellent Young Scholars (BK20240131), Natural Science Foundation of Jiangsu Province (BK20200677), and Joint Project of the Yangtze River Delta Science and Technology Innovation Community (2024CSJZN0600)

[#]Authors contributed equally to this work

*Corresponding authors, E-mail: yanliu@njmu.edu.cn; guox@njmu.edu.cn

LBP has demonstrated the ability to enhance neuronal proliferation, differentiation, and neurite outgrowth *in vitro* (Wang et al., 2018). Lycium barbarum glycopeptide (LbGp), a further refined and enriched extract, exhibits bioactivity that is 1–2 orders of magnitude stronger than LBP (Jiang et al., 2023). Studies have shown that LbGp increases pyramidal dendritic length *in vivo* (Dai et al., 2023) and confers neuroprotective, anticancer, and anti-aging effects (Chen et al., 2014; Lakshmanan et al., 2024; Xu et al., 2024). Notably, recent investigations have suggested that LbGp ameliorates depressive-like behaviors in rodent models subjected to chronic stress exposure (Dai et al., 2023; Fu et al., 2021). However, the precise effects and underlying mechanisms of LbGp in treating depression remain poorly understood, in part due to the lack of robust, disease-relevant human cellular models.

Gamma-aminobutyric acid (GABA), the primary inhibitory neurotransmitter in the central nervous system, plays a crucial role in modulating neuronal excitability, circuit homeostasis, and affective behaviors (Felice et al., 2022; Lydiard, 2003). Dysregulation of GABAergic signaling has been implicated in various neuropsychiatric disorders, including MDD (Della Vecchia et al., 2022). Animal models of MDD exhibit disrupted GABAergic signaling, characterized by reduced GABA synthesis, down-regulation of the GABA-synthesizing enzyme GAD67, and impaired function of both GABAA and GABAB receptors (Banasr et al., 2017; Jacobson et al., 2018; Luscher et al., 2011). Clinically, interventions aimed at restoring GABA levels, such as brexanolone (SAGE-547) and transcranial stimulation, have shown promise as antidepressants (Heimrath et al., 2020; Kanes et al., 2017). These findings underscore the therapeutic relevance of GABAergic dysfunction and support its utility as a pharmacological target in MDD. In a previous study, we established ventral forebrain organoids derived from MDD patients, which recapitulated key pathological features, including altered GABAergic neuronal morphology, increased neural firing, and dysregulated calcium signaling (Lu et al., 2023). These findings support the use of patient-derived ventral forebrain organoids as a robust platform for investigating candidate therapeutic interventions.

In this study, the effects of LbGp were evaluated in ventral forebrain organoids derived from MDD patients. LbGp treatment ameliorated abnormalities in neuronal morphology and functional activity. Bulk RNA sequencing (RNA-seq) identified increased endoplasmic reticulum (ER) stress in MDD organoids, including marked up-regulation of PERK, a key sensor of ER stress. To further explore the contribution of ER stress to MDD-associated phenotypes, control organoids were treated with the PERK activator CCT020312, which successfully replicated the neural deficits observed in MDD models. Notably, LbGp reversed CCT020312-induced alterations, indicating its capacity to modulate ER stress and restore neuronal function in MDD-associated models.

MATERIALS AND METHODS

Ethical approval

This study strictly followed the principles set out in the WMA Declaration of Helsinki and the Department of Health and Human Services Belmont Report. The human sample was collected with informed consent under full ethical approval in accordance with the Ethics Committee at Nanjing Medical University ([2024] No. 917).

Differentiation of induced pluripotent stem cells (iPSCs) into ventral forebrain organoids

iPSCs from a control individual (RC-A) and a patient diagnosed with MDD (SA006-1), matched for basic demographic characteristics, were used in this study. The cells were maintained in Essential 8 (E8, Life Technologies, USA) on vitronectin-coated plates (Life Technologies, USA). Routine passaging was performed using EDTA (Stemcell, Canada), with iPSC colonies incubated for 1 min and gently dissociated by pipetting two or three times. Medium was replenished daily by replacing half the volume with fresh E8. The protocol for ventral forebrain organoid differentiation followed our previously described methods (Liu et al., 2013; Yuan et al., 2020). Colonies were detached using dispase (1 U/mL, Life Technologies, USA) for 3 min to generate embryoid bodies (EBs), which were then transferred to neural induction medium (NIM) and cultured for 7 days. NIM, consisting of 500 mL Dulbecco's modified Eagle medium/nutrient mixture F-12 (DMEM/F12) supplemented with 5 mL N2 and 5 mL non-essential amino acids (NEAA), was supplemented with 10% fetal bovine serum (FBS) and used to facilitate the attachment of EBs onto six-well plates for an initial incubation period of 8 h. On day 7, the medium was replaced with serum-free NIM. Medium changes were performed every other day. From days 10 to 25, cultures were treated with 1 μmol/L sonic hedgehog agonist (SAG) to promote ventral patterning. Neural rosettes typically became visible by day 10. Rosette-containing colonies were gently dislodged using a 1 mL pipette and transferred to suspension culture in NIM supplemented with B27 (Life Technologies, USA). Organoids were enzymatically dissociated into single neurons using TrypLE (Life Technologies, USA), with samples co-incubated for 7 min. The resulting cells were plated at a density of 30 000–50 000 cells/cm² onto coverslips pre-coated with poly-L-ornithine (Sigma, USA) and Matrigel (BD Biosciences, USA) for morphological analysis. Organoids and dissociated neurons were subsequently used for immunostaining, calcium imaging, and electrophysiological recording.

Immunocytochemistry

Organoids were fixed on day 45 in 4% paraformaldehyde (PFA) in phosphate-buffered saline (PBS) for 4 h at 4°C. Following fixation, samples were cryoprotected by sequential incubation in 20% and then 30% sucrose solutions, each for 24 h. Cryosectioning was performed using a cryotome. Tissue sections were washed three times in PBS, 10 minutes per wash, and subsequently blocked and permeabilized in a solution containing 5% donkey serum (MilliporeSigma, USA) and 1% Triton X-100 (Bio-Link, China). Sections were incubated overnight at 4°C with primary antibodies diluted in 5% donkey serum and 0.2% Triton X-100. The following day, slides were washed three times in PBS and incubated for 1 h at room temperature in secondary antibodies diluted in 5% donkey serum and PBS. After an additional three PBS washes, slides were coated with mounting medium (Fluoromount-G, SouthernBiotech, USA) and covered with cover glass for fluorescence imaging. Images were acquired using an Eclipse 80i fluorescence microscope (Nikon, Japan).

Whole-cell patch-clamp recordings

Whole-cell patch-clamp recordings were performed on GABAergic interneurons at 6–8 weeks. Neurons were visualized using an Olympus microscope (Japan), and signals

were digitized with a Digidata 1550B interface and acquired using Axon MultiClamp 700B differential amplifier (USA). Data acquisition and analyses were performed using Axon Clampex software (Molecular Devices, USA). Coverslips were transferred to an external solution containing 119 μmol/L NaCl, $CaCl_2$ (1 mmol/L), KCL (5 mmol/L), $MgCl_2$ (1 mmol/L), HEPES (5 mmol/L), and glucose (5 mmol/L, 280 mosM, pH 7.3). Patch pipettes (resistance 7–12 MΩ) were filled with internal recording solution containing 130 mmol/L K-gluconate, KCl (10 mmol/L), $MgCl_2$ (2 mmol/L), Na-GTP (0.3 mmol/L), Na-ATP (2 mmol/L), EGTA (10 mmol/L), and HEPES (10 mmol/L, 280 mosM, pH 7.3). Neurons were held at −70 mV in current-clamp mode and action potentials (APs) were induced by injecting stepwise current pulses (10 steps, 10 pA increments). Voltage and current signals were recorded using the same amplifier and Digidata 1322A interface, and data were analyzed using Clampfit (USA). All recordings were performed at room temperature.

Calcium imaging

Ventral forebrain organoids were plated onto Matrigel-coated confocal dishes and prepared for calcium imaging. Organoids were incubated with Fluo-4 AM (Life Technologies, USA) for 20 min at 37°C, followed by an additional 20 min of incubation at room temperature, After a single wash with DPBS (Life Technologies, USA), the medium was replaced with live-cell imaging solution. Calcium imaging was performed on a Zeiss LSM 900 confocal microscope (Germany) equipped with a 20× objective, using 488 nm excitation. Time-series images were acquired at a speed of one frame every 3.2 s. At the fifth frame, organoids were stimulated with a high-KCL solution (67 mmol/L). Image analysis was performed using GraphPad Prism v.8 and ImageJ. Single-cell calcium activity was quantified by calculating the peak fluorescence ratio, (Fmax–F0)/F0, where F0 represents the initial fluorescence intensity.

Bulk RNA-seq analysis

Total RNA was extracted using TRIzol reagent (Life Technologies, USA), and mRNA was enriched using oligo(dT) magnetic beads. Enriched mRNA was reverse-transcribed into cDNA, and RNA sequencing and library construction was performed using the Illumina HiSeq™ 2500 platform (USA). Differential gene expression analysis was performed using the DESeq2 package (v.1.30.0). Volcano plots illustrating up-regulated and down-regulated genes were generated using the Enhanced Volcano package (v.1.10.0). Reactome pathway enrichment analysis was performed using the Reactome online tool. Kyoto Encyclopedia of Genes and Genomes (KEGG) pathway and Gene Ontology (GO) enrichment analyses were performed using the clusterProfiler package (v.4.0.2). Gene expression patterns within selected enriched terms were visualized using the pheatmap package (v.1.0.12). Enrichment terms with $P<0.05$ were considered statistically significant. Drug-protein interaction networks were analyzed using the NetworkAnalyst platform, incorporating data from the DrugBank database.

Statistical analysis

Unpaired *t*-test was used for comparisons between two independent groups, while one-way analysis of variance (ANOVA) or Kruskal-Wallis test was applied when comparing more than two groups. All statistical analyses were performed using GraphPad Prism v.8, with $P<0.05$ considered statistically significant.

RESULTS

MDD-derived ventral forebrain organoids exhibit aberrant GABAergic neuronal morphology and activity

Ventral forebrain organoids were generated using a previously established method (Lu et al., 2023) (Figure 1A). After 35 days of continuous culture, organoids displayed stratified neuroepithelium-like architecture and expressed the neural progenitor markers Ki67 and SOX2, as well as the neuronal marker TUJ1. Further characterization revealed robust expression of the ventral progenitor marker NKX2.1, with comparable proportions observed in control and MDD-derived groups (Ctrl: 65.56%±1.80%, MDD: 65.89%±2.01%). By day 39, both groups expressed GABAergic neuronal markers GABA, calretinin, and calbindin. Expression of the mature GABAergic neuronal marker GAD67 (Ctrl: 79.25%±2.01%, MDD: 77.50%±1.63%) confirmed the presence of differentiated GABAergic interneurons (Figure 1B; Supplementary Figure S1A, B).

To assess the suitability of MDD-derived ventral forebrain organoids for therapeutic screening, organoids were treated with 10 μmol/L brain-derived neurotrophic factor (BDNF) for 14 days from day 25. BDNF is known to exert neuroprotective and antidepressant effects (Cavaleri et al., 2023; Szuhany & Otto, 2020). Morphological assessment on day 40 revealed significant differences between Ctrl and MDD-derived groups. Sholl analysis showed no significant changes in the morphological complexity between Ctrl and BDNF-treated Ctrl groups (Supplementary Figure S1C). In contrast, BDNF-treated MDD neurons exhibited significantly reduced primary neurite length compared to untreated MDD neurons (Figure 1D). Furthermore, the number of primary and secondary neuritic branches, as well as the number of intersections within concentric zones at 10 and 20 μm from the soma, were reduced following BDNF treatment (Figure 1E; Supplementary Figure S1D), indicating partial rescue of morphological defects in MDD GABAergic interneurons.

To assess functional activity, calcium imaging was performed using Fluo-4 AM on day 39. Calcium imaging is considered a reliable method for studying neuronal activity and neural circuits (Chen et al., 2013). Time-lapse confocal microscopy captured dynamic intracellular calcium transients in response to 67 mmol/L KCL stimulation. Quantification of fluorescence amplitude (Fmax–F0)/F0, which reflects the amplitude of calcium signaling, revealed attenuated calcium responses in MDD-derived GABAergic interneurons, which were significantly enhanced following BDNF treatment (Figure 1F, G). Electrophysiological analysis was conducted on 6-week-old organoids using whole-cell patch-clamp recordings. Under voltage-clamp conditions, APs were evoked by current injections ranging from 10 to 60 pA. Compared with the Ctrl group, AP amplitudes and number of evoked APs were higher in the MDD group, while the half-width of the first AP was decreased. Importantly, BDNF treatment restored these neuronal defects in MDD GABAergic interneurons (Figure 1H, I).

Taken together, these results demonstrate that BDNF treatment partially reverses aberrant neuronal morphology, calcium signaling, and hyperactivity in MDD-derived ventral forebrain organoids. This organoid model recapitulates key pathological features of MDD and provides a robust platform

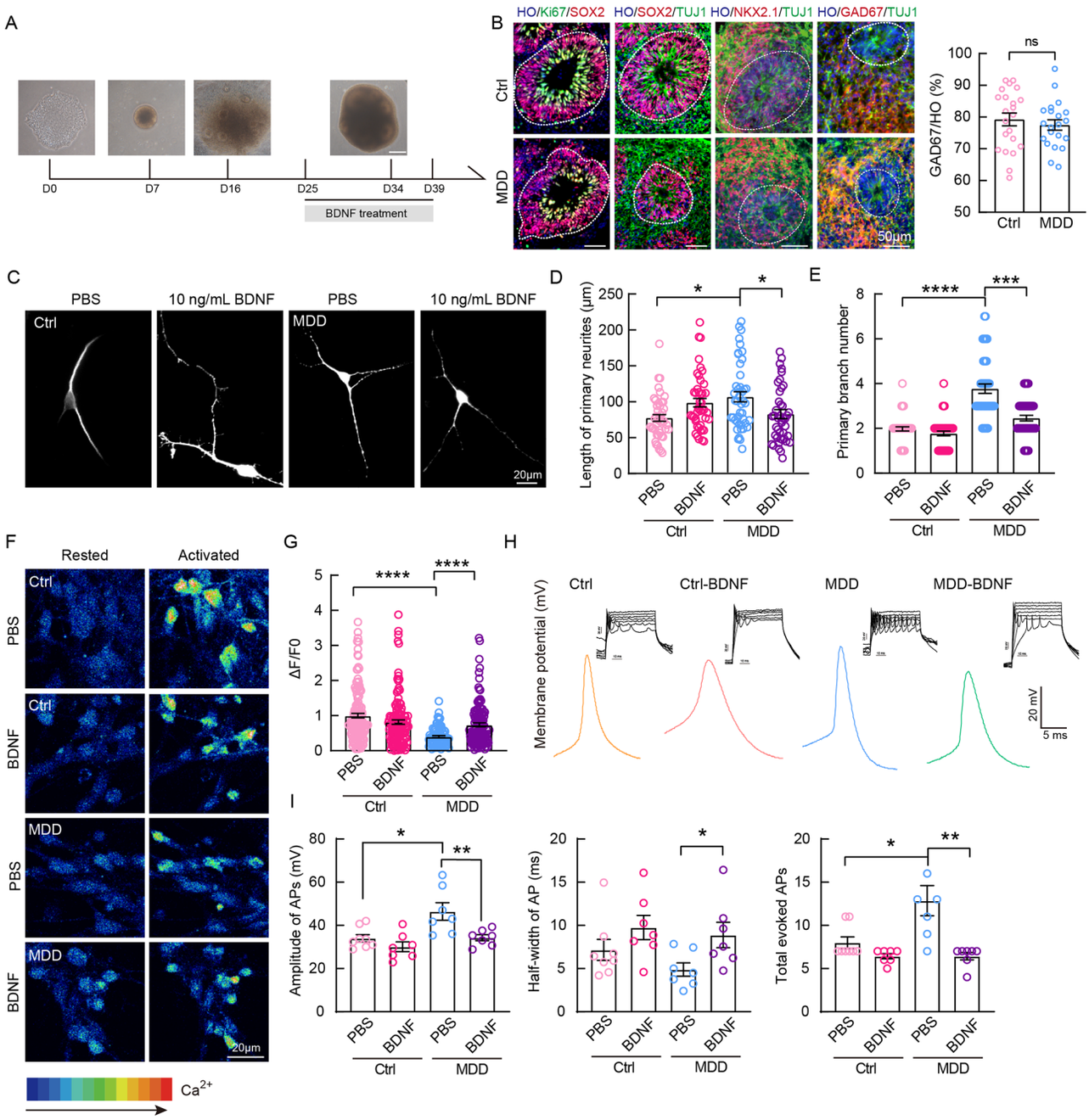

Figure 1 Differentiation of MDD-derived ventral forebrain organoids and effects of BDNF treatment

A: Schematic overview of the protocol used for generating ventral forebrain organoids. Scale bar: 250 μm. B: Immunofluorescence staining for the proliferation marker Ki67, neural progenitor marker SOX2, ventral prosencephalic progenitor marker NKX2.1, and GABA interneuron marker GAD67. Quantification of GAD67 expression. *t*-test, Mean±SEM. C: Representative images of GABAergic interneurons from each group on day 39. D: Quantification of primary neurite lengths on day 39. $n \geq 60$, Kruskal-Wallis H test (nonparametric), *: $P<0.05$; **: $P<0.01$. Mean±SEM. E: Quantification of primary branch numbers on day 39. $n \geq 60$, Kruskal-Wallis test (nonparametric), ***: $P<0.001$; ****: $P<0.0001$. Mean±SEM. F: Representative time-lapse images of calcium transients across groups. G: Quantification of peak calcium amplitude, calculated as (Fmax–F0)/F0, per group. Kruskal-Wallis test (nonparametric), ****: $P<0.0001$. Mean±SEM. H: Representative whole-cell patch-clamp recordings showing evoked APs at a holding potential of 70 mV. I: Quantification of AP amplitude, half width of the first AP evoked by 10 pA current injection, and total number of evoked APs per group. One-way ANOVA, *: $P<0.05$; **: $P<0.01$. Mean±SEM.

for evaluating candidate therapeutic interventions.

LbGp treatment restores abnormal GABAergic neuronal morphology and activity

To determine the optimal working concentration of LbGp, ventral forebrain organoids were exposed to varying concentrations of LbGp (0, 1, 10, 100, 500 μg/mL, 1, 2 mg/mL) for 15 days. Organoids treated with 1 or 2 mg/mL were surrounded by clusters of dead cells (Supplementary Figure S2A), suggesting cytotoxicity at these doses. Cellular cytotoxicity assessed using the CCK-8 assay confirmed a significant reduction in cell viability in the 1 mg/mL group, indicating a cytotoxic threshold at or above this concentration (Supplementary Figure S2B).

To further evaluate LbGp-induced cytotoxicity, cleaved

caspase-3 expression was quantified as a marker of apoptosis. Caspase-3 is a key effector of apoptosis execution, with proteolytic activity that cleaves cellular substrates leading to programmed cell death in response to extrinsic or intrinsic apoptotic signals (Huang et al., 2011). Results showed a remarkable increase in caspase-3 activity in the organoids treated with 1 or 2 mg/mL LbGp (Ctrl: 9.32%±0.98%, 500 μg/mL: 12.36%±0.85%, 1 mg/mL: 14.57±0.68%, 2 mg/mL: 16.37%±0.83%) (Supplementary Figure S2C), indicating enhanced apoptotic activity at these concentrations. Correspondingly, quantification of fragmented cells—indicative of late-stage apoptosis—revealed a higher incidence in the 1 and 2 mg/mL LbGp groups (Ctrl: 9.41%±1.36%, 500 μg/mL: 8.46%±0.68%, 1 mg/mL: 16.32%±1.114%, 2 mg/mL: 15.92%±1.16%) (Supplementary Figure S2D), further highlighting the pro-apoptotic effects of LbGp at these concentrations. Based on these findings, concentrations of 0, 10, 100, and 500 μg/mL were selected for further experiments, as they demonstrated minimal cytotoxicity while still allowing assessment of therapeutic efficacy. Consequently, doses exceeding 500 μg/mL were excluded from further analysis.

To investigate the potential therapeutic impact of LbGp on MDD-associated phenotypes, both control and MDD-derived organoids were treated with various concentrations of LbGp (0, 1, 10, 100, and 500 μg/mL) for 14 days (Figure 2A). After treatment, notable improvements in neuronal morphology were observed, particularly in the 500 μg/mL MDD group, including significant reductions in the lengths of the longest and second-longest neurites (Figure 2B, C). Morphometric analysis further revealed a marked decrease in the number of primary and secondary neurites in the 500 μg/mL group (Figure 2D), along with reduced neuritic intersections at radial distances of 10 and 20 μm from the soma (Figure 2E). These findings suggest that LbGp treatment, particularly at 500 μg/mL, partially restores the structural abnormalities of GABAergic neurons in MDD organoids.

To further explore the potential role of LbGp in ameliorating dysfunctional neuronal activity, intracellular calcium dynamics were assessed using Fluo-4 AM. Results showed that MDD-derived organoids displayed attenuated calcium transients, which were significantly increased following LbGp treatment (Figure 2F, G), suggesting a functional recovery in calcium signaling. Given the concurrent restoration of neuronal morphology and calcium activity at the 500 μg/mL dose, the impact of LbGp on GABAergic neuron excitability was next examined using whole-cell patch-clamp electrophysiology. After two weeks of LbGp treatment, the first evoked AP in the MDD organoids was reduced (Figure 2H), indicating attenuation of neuronal hyperexcitability, a hallmark feature of MDD-related neural dysfunction (Lu et al., 2023).

Collectively, these findings demonstrate that treatment with 500 μg/mL LbGp effectively reverses several pathological features of MDD, including abnormal neuronal morphology, impaired calcium signaling, and hyperactive electrical activity. These results highlight the potential therapeutic effects of LbGp in modulating both neuronal structure and function in MDD.

Bulk RNA-seq reveals LbGp treatment reverses ER stress dysregulation in MDD

To elucidate the potential mechanisms by which LbGp ameliorates MDD-associated pathology, bulk RNA-seq was performed on four experimental groups: Ctrl, LbGp-treated Ctrl, MDD, and LbGp-treated MDD (Figure 3A). Based on its efficacy in previous phenotypic assays, the 500 μg/mL LbGp concentration showed the most potent therapeutic effects and was thus selected for further transcriptomic profiling. Principal component analysis (PCA) revealed that the LbGp-treated MDD group clustered more closely with both Ctrl groups, suggesting that LbGp treatment partially restored global gene expression patterns toward a control-like state (Figure 3B).

Differential expression analysis identified 838 up-regulated and 879 down-regulated genes in MDD compared with Ctrl (Figure 3C). GO enrichment analysis highlighted significant up-regulation of ER stress-related pathways in the MDD group, particularly those associated with the unfolded protein response (Figure 3D). In contrast, comparison between LbGp-treated MDD and untreated MDD groups revealed 810 up-regulated and 790 down-regulated genes (Figure 3E). GO enrichment analysis showed that ER stress-associated pathways were down-regulated in the LbGp-treated MDD group (Figure 3F), suggesting that LbGp regulates ER stress in this disease context.

Hierarchical clustering and heatmap visualization further demonstrated that the global gene expression profile of LbGp-treated MDD organoids resembled that of the Ctrl group (Figure 3G). Among the differentially expressed genes (DEGs), 578 were up-regulated in MDD compared to the Ctrl and subsequently down-regulated following LbGp treatment (Figure 3H). Notably, many of these genes were associated with ER stress, particularly those involved in protein folding (Figure 3I). The PERK-mediated unfolded protein response—a central regulator of ER stress—was significantly altered in MDD organoids (Figure 3J).

Key ER stress markers, including *DDIT3*, *EIF2S1*, and *HSPA5*, were found to be dysregulated in MDD. Real time quantitative PCR (RT-qPCR) validated these transcriptomic findings, confirming up-regulation of ER stress markers in MDD and down-regulation following LbGp treatment (Figure 3K–M). These results implicate ER stress suppression as a likely mechanism through which LbGp confers therapeutic benefit.

To further investigate the effects of ER stress activation, genes associated with GABAergic neuronal function was analyzed. ER stress is known to influence both protein synthesis and AP regulation (Bahar et al., 2016; Ghemrawi & Khair, 2020). Several genes essential for GABA synthesis and function, such as *ABAT* and *CALB1*, were down-regulated in MDD but up-regulated following LbGp treatment. Similarly, genes related to membrane excitability also exhibited differential expression across the Ctrl, MDD, and LbGp-treated MDD groups, indicating that LbGp may play a role in regulating both GABA biosynthesis and membrane excitability in MDD.

Together, these findings suggest that LbGp may mitigate MDD-associated ER stress by regulating key molecular pathways, offering insights into its potential as a therapeutic strategy for addressing ER stress-related pathologies in MDD.

LbGp ameliorates aberrant GABAergic neuronal morphology and activity via ER stress suppression

To investigate whether the therapeutic effects of LbGp on MDD-associated phenotypes are mediated through the modulation of ER stress, organoids from the control group were treated with 10 μmol/L CCT020312, a selective activator of the PERK pathway. This concentration has been previously

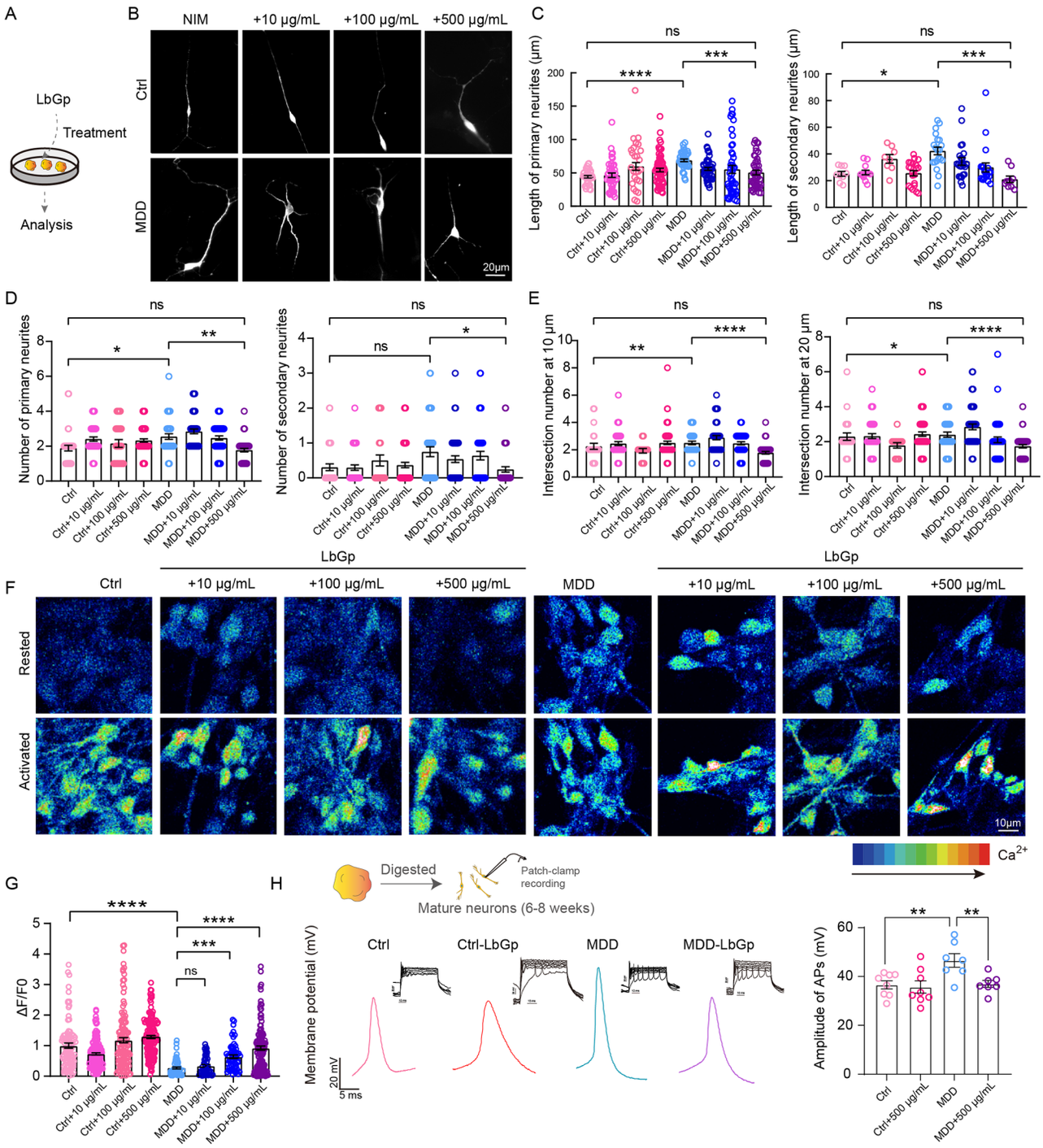

Figure 2 LbGp treatment restores aberrant neuronal morphology and activity in MDD-derived organoids

A: Schematic illustration of the experimental design for LbGp treatment. B: Representative images of GABAergic interneurons from each group on day 39. C: Quantification of primary and secondary neurite lengths on day 39. $n \geq 60$, Kruskal-Wallis test (nonparametric), *: $P<0.05$; **: $P<0.01$. Mean±SEM. D: Quantification of primary and secondary branch numbers on day 39. $n \geq 60$, Kruskal-Wallis test (nonparametric), ****: $P<0.0001$. Mean±SEM. E: Quantification of neurite intersection numbers at 10 μm and 20 μm from the central soma. Kruskal-Wallis test (nonparametric), **: $P<0.01$; ****: $P<0.0001$. Mean±SEM. F: Representative time-lapse images of calcium transients across groups. G: Quantification of peak calcium amplitude, calculated as (Fmax–F0)/F0, per group. Kruskal-Wallis test (nonparametric), *: $P<0.05$; ****: $P<0.0001$. Mean±SEM. H: Representative whole-cell patch-clamp recordings showing APs at a holding potential of 70 mV. Quantification of first AP amplitude following 10 pA current injection. One-way ANOVA, **: $P<0.01$. Mean±SEM.

validated as an effective working concentration (Lei et al., 2021; Stockwell et al., 2012). Following treatment for 7 and 10 days, calcium imaging revealed a significant reduction in neuronal activity in the MDD organoids, while shorter treatment durations produced no notable effect (Figure 4A), Based on these findings, a 7 days treatment regime was selected for the following experiments.

To determine the morphological consequences of PERK activation, GABAergic neuron structure was assessed following CCT020312 treatment. Treated neurons exhibited a

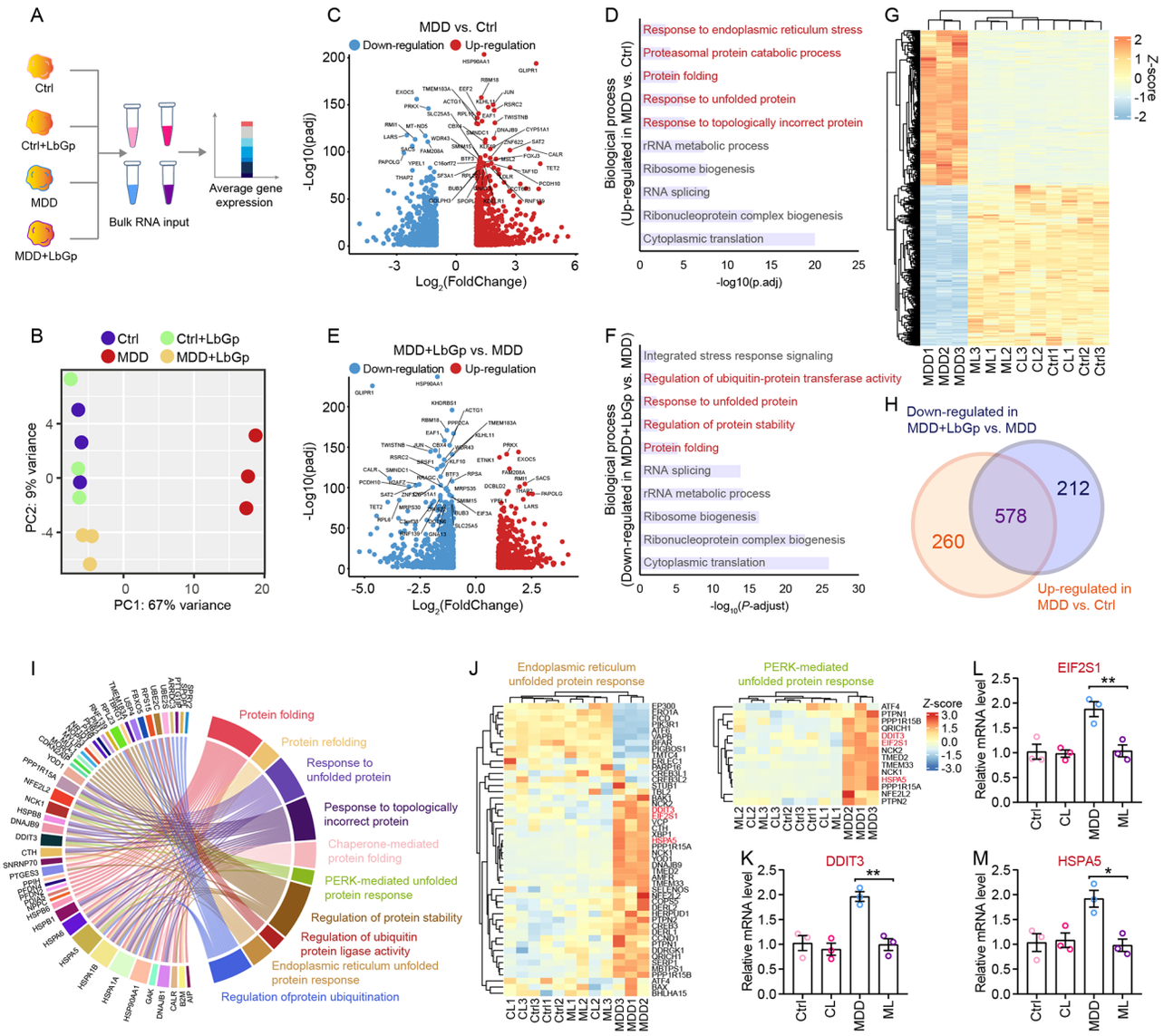

Figure 3 Bulk RNA-seq analysis revealed LbGp mitigated ER stress in MDD

A: Schematic representation of bulk RNA-seq of ventral forebrain organoids on day 39. B: PCA of different groups. C: Volcano plot showing differentially expressed genes (DEGs) in MDD organoids compared with Ctrl group. D: GO analysis of DEGs between Ctrl and MDD organoids. E. olcano plot showing differentially expressed genes (DEGs) in LbGp-treated MDD organoids compared with MDD group. F: Volcano plot showing DEGs in LbGp-treated MDD organoids compared with MDD organoids. G: GO analysis of DEGs between LbGp-treated MDD organoids (ML) and MDD organoids. CL: LbGp-treated Ctrl organoids. H: Heatmap of DEGs in different groups. I: Overlap analysis showing number of down-regulated genes in LbGp-treated MDD organoids compared with MDD organoids, and up-regulated genes in MDD organoids compared with Ctrl organoids. J: GO analysis of overlapping down-regulated genes in LbGp-treated MDD organoids and MDD organoids, and up-regulated genes in MDD organoids compared with Ctrl organoids. K: Heatmap showing expressed genes related to ER stress and PERK-mediated unfolded protein response in different groups. L: RT-qPCR quantification of relative DDIT3 expression in different groups. *t*-test, **: P<0.01. Mean±SEM. M: RT-qPCR quantification of relative EIF2S1 expression in different groups. *t*-test, **: P<0.01. Mean±SEM. N: RT-qPCR quantification of relative HSPA5 expression in different groups. *t*-test, **: P<0.01. Mean±SEM.

significant increase in neurite length (Ctrl: 76.44±5.06 μm; Ctrl+CCT020312:94.77±3.75 μm) and a marked increase in the number of neuronal branches (Figure 4B), indicating that prolonged ER stress activation alters neuronal development in a manner consistent with MDD-like phenotypes.

To determine whether LbGp alleviates ER stress-induced abnormalities in neuronal morphology and activity, organoids were co-treated with CCT020312 and LbGp for 7 days. Combined treatment significantly reduced both neurite length and the number of primary branches relative to the CCT020312-only group (Figure 4C), suggesting that LbGp effectively rescues the phenotypic alterations induced by ER stress activation. Functional assays using Fluo-4 calcium imaging and whole-cell patch-clamp recordings further revealed that neuronal activity, which was suppressed by CCT020312, was significantly restored following LbGp co-treatment (Figure 4D, E), indicating that LbGp not only improves neuronal morphology but also restores neuronal activity by mitigating ER stress.

Collectively, these findings provide strong evidence that LbGp rescues neuronal morphology and activity through the alleviation of ER stress, offering a potential therapeutic

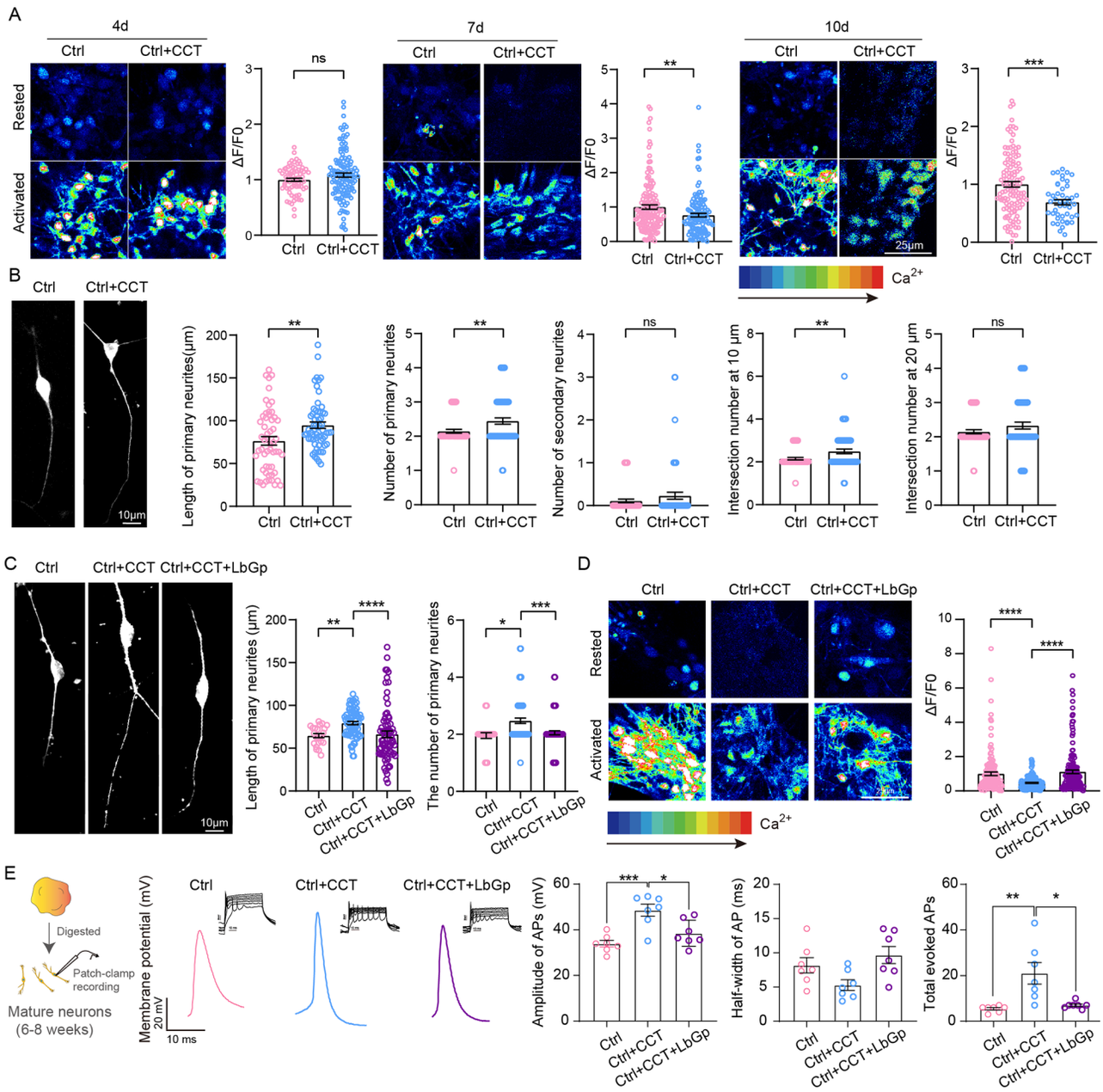

Figure 4 LbGp restores aberrant neuronal morphology and activity after CCT020312 treatment

A: Representative time-lapse calcium transients across groups, and quantification of peak intracellular calcium amplitude, calculated as (Fmax–F0)/F0, per group. *t*-test, **: $P<0.01$; ***: $P<0.001$. Mean±SEM. B: Representative images of GABAergic interneurons on day 35. Quantification of neurite length and number. Quantification of neurite intersection number at 10 μm and 20 μm from the central soma. *t*-test, **: $P<0.001$. Mean±SEM. C: Representative images of GABAergic interneurons on day 35. Quantification of neurite length and number. Kruskal-Wallis test (nonparametric), *: $P<0.05$; **: $P<0.01$; ***: $P<0.001$; ****: $P<0.0001$. Mean±SEM. D: Representative time-lapse calcium transients across groups, and quantification of peak intracellular calcium amplitude, calculated as (Fmax–F0)/F0, per group. Kruskal-Wallis test (nonparametric), ****: $P<0.0001$. Mean±SEM. E: Representative whole-cell patch-clamp recordings showing APs at a holding potential of 70 mV. Quantification of amplitude and half-width of first AP generated in response to 10 pA current injection. Quantification of total evoked APs per group. One-way ANOVA, **: $P<0.01$. Mean±SEM.

strategy for MDD-associated neuronal dysfunction.

DISCUSSION

MDD is a heterogeneous psychiatric condition with limited diagnostic and therapeutic options. Several natural plant-derived compounds have been shown to alleviate depressive-like phenotypes, with mechanisms often attributed to their ability to repair the brain microenvironment —reducing neuroinflammation, oxidative stress, and apoptotic signaling (Wu et al., 2015);(Liu et al., 2024; Pan et al., 2023). For example, *Lepidium meyenii* (maca) enhances the efficacy of selective serotonin reuptake inhibitors (SSRIs) (Dording et al., 2008); *Withania somnifera* (ashwagandha) exhibits significant anti-stress and anti-anxiety effects via modulation of GABAergic and serotonergic pathways (Speers et al., 2021); and saffron extract alleviates depression and anxiety by modulating serotonergic and dopaminergic neurotransmission (Pachikian et al., 2021). The present study identified a

previously unrecognized role of LbGp, a purified wolfberry extract, in modulating MDD-related phenotypes through regulation of ER stress in human ventral forebrain organoids.

ER stress plays a fundamental role in cellular proteostasis, calcium homeostasis, and excitability regulation via the PERK signaling pathway (Bahar et al., 2016; Wang et al., 2024; Wu et al., 2019). Consistent with this, our results demonstrated that ER stress activation through CCT020312 altered calcium transients and electrophysiological activity in GABAergic neurons. ER stress has been implicated in the pathophysiology of depression (Mao et al., 2019), with evidence from chronic unpredictable mild stress (CUMS) murine models linking depressive-like behaviors to ER stress, mitochondrial dysfunction, ATP depletion, oxidative imbalance, and neuronal apoptosis (Liu et al., 2011). Additionally, honokiol, a compound isolated from *Magnolia officinalis* bark, has been shown to alleviate chronic stress-induced depressive-like behavior by preventing ER stress in the hippocampus of mice (Tan et al., 2015). Chronic social defeat stress has also been found to activate the PERK-eIF2α signaling pathway in the hippocampus, leading to BDNF down-regulation and behavioral and memory impairments in mice (Li et al., 2019). In our organoid model, bulk RNA-seq revealed up-regulation of ER stress markers, including components of the PERK-eIF2α signaling pathway, which were significantly down-regulated following LbGp treatment.

ER stress is closely linked to oxidative stress, largely mediated by the accumulation of reactive oxygen species (ROS) (Verfaillie et al., 2012). LbGp possesses intrinsic antioxidant properties that may attenuate ER stress by scavenging ROS and preserving redox homeostasis (Zhao et al., 2005). By reducing oxidative stress, LbGp likely helps maintain proper protein folding within the ER, preventing misfolding and aggregation —processes implicated in depressive pathology. These findings provide mechanistic insight into how LbGp ameliorates MDD-associated cellular dysfunction in a human-relevant model.

Previous studies have consistently reported structural, functional, and neurochemical deficits in the GABAergic system in both animal models and individuals with depression (Duman et al., 2019). Specifically, reductions in GABA levels during the later stages of MDD have been associated with increased neuronal excitability and vulnerability to cell death (Ashpole et al., 2012), and postmortem studies have identified altered neuronal densities of GABAergic neurons in affected brain regions (Macqueen et al., 2008). These findings underscore the central role of GABAergic dysfunction in MDD pathophysiology. In this context, our study utilized patient-derived ventral forebrain organoids to assess the therapeutic potential of LbGp in restoring GABAergic neuronal structure and function, further supporting its relevance as a candidate antidepressant compound.

CONCLUSIONS

This study established a human-derived ventral forebrain organoid model as an effective platform for probing MDD-associated cellular pathology and evaluating candidate therapeutics. Using this system, LbGp was shown to reverse MDD-related neuronal dysfunction by suppressing ER stress signaling, highlighting a distinct molecular pathway underlying its therapeutic potential.

DATA AVAILABILITY

All RNA sequencing data were deposited in the National Center for Biotechnology Information (NCBI) database (GSE285923), Genome Sequence Archive (PRJCA039110, HRA011220), and Science Data Bank (DOI: https://doi.org/10.57760/sciencedb.j00139.00207).

SUPPLEMENTARY DATA

Supplementary data to this article can be found online.

COMPETING INTERESTS

The authors declare that they have no competing interests.

AUTHORS' CONTRIBUTIONS

M.D.T.: Data curation; investigation; writing-original draft; project administration; formal analysis; writing-review and editing. C.W.: Investigation; methodology. X.H.W.: Data curation; software; formal analysis; investigation. Q.C.: Data curation; software; investigation; formal analysis. W.W.G.: Data curation; investigation; formal analysis. M.X.: Investigation; methodology. Y.H.: Investigation; methodology. X.H.: Funding acquisition; writing-review and editing. W.Y.Z.: Funding acquisition; writing-review and editing. Q.Z.: Funding acquisition; writing-review and editing. X.G.: Funding acquisition; project administration; writing-original draft; writing-review and editing. Y.L.: Supervision; project administration; funding acquisition; writing-original draft; writing-review and editing. All authors read and approved the final version of the manuscript.

REFERENCES

Anderson E, Crawford CM, Fava M, et al. 2024. Depression - understanding, identifying, and diagnosing. *The New England Journal of Medicine*, **390**(17): e41.

Ashpole NM, Song WH, Brustovetsky T, et al. 2012. Calcium/calmodulin-dependent protein kinase II (CaMKII) inhibition induces neurotoxicity via dysregulation of glutamate/calcium signaling and hyperexcitability. *Journal of Biological Chemistry*, **287**(11): 8495–8506.

Bahar E, Kim H, Yoon H. 2016. ER stress-mediated signaling: action potential and Ca^{2+} as key players. *International Journal of Molecular Sciences*, **17**(9): 1558.

Banasr M, Lepack A, Fee C, et al. 2017. Characterization of GABAergic marker expression in the chronic unpredictable stress model of depression. *Chronic Stress (Thousand Oaks)*, **1**: 2470547017720459.

Cavaleri D, Moretti F, Bartoccetti A, et al. 2023. The role of BDNF in major depressive disorder, related clinical features, and antidepressant treatment: insight from meta-analyses. *Neuroscience & Biobehavioral Reviews*, **149**: 105159.

Chen TW, Wardill TJ, Sun Y, et al. 2013. Ultrasensitive fluorescent proteins for imaging neuronal activity. *Nature*, **499**(7458): 295–300.

Chen WW, Cheng X, Chen JZ, et al. 2014. *Lycium barbarum* polysaccharides prevent memory and neurogenesis impairments in scopolamine-treated rats. *PLoS One*, **9**(2): e88076.

Cuijpers P, Gentili C, Banos RM, et al. 2016. Relative effects of cognitive and behavioral therapies on generalized anxiety disorder, social anxiety disorder and panic disorder: a meta-analysis. *Journal of Anxiety Disorders*, **43**: 79–89.

Dai YL, Guo JX, Zhang BR, et al. 2023. Lycium barbarum (Wolfberry) glycopeptide prevents stress-induced anxiety disorders by regulating oxidative stress and ferroptosis in the medial prefrontal cortex. *Phytomedicine*, **116**: 154864.

Della Vecchia A, Arone A, Piccinni A, et al. 2022. GABA system in depression: impact on pathophysiology and psychopharmacology. *Current Medicinal Chemistry*, **29**(36): 5710–5730.

Dietz BM, Hajirahimkhan A, Dunlap TL, et al. 2016. Botanicals and their bioactive phytochemicals for women's health. *Pharmacological Reviews*, **68**(4): 1026–1073.

Dording CM, Fisher L, Papakostas G, et al. 2008. A double-blind, randomized, pilot dose-finding study of maca root (L. meyenii) for the management of SSRI-induced sexual dysfunction. *CNS Neuroscience & Therapeutics*, **14**(3): 182–191.

Duman RS, Sanacora G, Krystal JH. 2019. Altered connectivity in depression: GABA and glutamate neurotransmitter deficits and reversal by novel treatments. *Neuron*, **102**(1): 75–90.

Felice D, Cryan JF, O'Leary OF. 2022. $GABA_B$ receptors: anxiety and mood disorders. *Current Topics in Behavioral Neurosciences*, **52**: 241–265.

Fu YW, Peng YF, Huang XD, et al. 2021. Lycium barbarum polysaccharide-glycoprotein preventative treatment ameliorates aversive stimuli-induced depression. *Neural Regeneration Research*, **16**(3): 543–549.

Ghemrawi R, Khair M. 2020. Endoplasmic reticulum stress and unfolded protein response in neurodegenerative diseases. *International Journal of Molecular Sciences*, **21**(17): 6127.

Heimrath K, Brechmann A, Blobel-Lüer R, et al. 2020. Transcranial direct current stimulation (tDCS) over the auditory cortex modulates GABA and glutamate: a 7 T MR-spectroscopy study. *Scientific Reports*, **10**(1): 20111.

Huang Q, Li F, Liu XJ, et al. 2011. Caspase 3-mediated stimulation of tumor cell repopulation during cancer radiotherapy. *Nature Medicine*, **17**(7): 860–866.

Jacobson LH, Vlachou S, Slattery DA, et al. 2018. The gamma-aminobutyric acid B receptor in depression and reward. *Biological Psychiatry*, **83**(11): 963–976.

Janda K, Wojtkowska K, Jakubczyk K, et al. 2020. *Passiflora incarnata* in neuropsychiatric disorders-a systematic review. *Nutrients*, **12**(12): 3894.

Jiang ZF, Zeng Z, He H, et al. 2023. Lycium barbarum glycopeptide alleviates neuroinflammation in spinal cord injury via modulating docosahexaenoic acid to inhibiting MAPKs/NF-kB and pyroptosis pathways. *Journal of Translational Medicine*, **21**(1): 770.

Kanes S, Colquhoun H, Gunduz-Bruce H, et al. 2017. Brexanolone (SAGE-547 injection) in post-partum depression: a randomised controlled trial. *The Lancet*, **390**(10093): 480–489.

Lakshmanan Y, Wong FSY, So KF, et al. 2024. Lycium barbarum glycopeptide promotes neuroprotection in ET-1 mediated retinal ganglion cell degeneration. *Journal of Translational Medicine*, **22**(1): 727.

Lei YP, He LR, Yan C, et al. 2021. PERK activation by CCT020312 chemosensitizes colorectal cancer through inducing apoptosis regulated by ER stress. *Biochemical and Biophysical Research Communications*, **557**: 316–322.

Li MX, Li Q, Sun XJ, et al. 2019. Increased Homer1-mGluR5 mediates chronic stress-induced depressive-like behaviors and glutamatergic dysregulation via activation of PERK-eIF2α. *Progress in Neuro-Psychopharmacology and Biological Psychiatry*, **95**: 109682.

Liu YN, Yang C, Zhang JY, et al. 2024. Recent progress in adverse events of carboxylic acid non-steroidal anti-inflammatory drugs (CBA-NSAIDs) and their association with the metabolism: the consequences on mitochondrial dysfunction and oxidative stress, and prevention with natural plant extracts. *Expert Opinion on Drug Metabolism & Toxicology*, **20**(8): 765–785.

Liu YY, Yang N, Hao WY, et al. 2011. Dynamic proteomic analysis of protein expression profiles in whole brain of Balb/C mice subjected to unpredictable chronic mild stress: implications for depressive disorders and future therapies. *Neurochemistry International*, **58**(8): 904–913.

Lu KQ, Hong Y, Tao MD, et al. 2023. Depressive patient-derived GABA interneurons reveal abnormal neural activity associated with HTR2C. *EMBO Molecular Medicine*, **15**(1): e16364.

Luscher B, Shen Q, Sahir N. 2011. The GABAergic deficit hypothesis of major depressive disorder. *Molecular Psychiatry*, **16**(4): 383–406.

Lydiard RB. 2003. The role of GABA in anxiety disorders. *The Journal of Clinical Psychiatry*, **64 Suppl 3**: 21–27.

Macqueen GM, Yucel K, Taylor VH, et al. 2008. Posterior hippocampal volumes are associated with remission rates in patients with major depressive disorder. *Biological Psychiatry*, **64**(10): 880–883.

Mao JX, Hu YR, Ruan LM, et al. 2019. Role of endoplasmic reticulum stress in depression (review). *Molecular Medicine Reports*, **20**(6): 4774–4780.

Pachikian BD, Copine S, Suchareau M, et al. 2021. Effects of saffron extract on sleep quality: a randomized double-blind controlled clinical trial. *Nutrients*, **13**(5): 1473.

Pan J, Lu YT, Wang SJ, et al. 2023. Synergistic neuroprotective effects of two natural medicinal plants against CORT-induced nerve cell injury by correcting neurotransmitter deficits and inflammation imbalance. *Phytomedicine*, **121**: 155102.

Rakel RE. 1999. Depression. *Primary Care: Clinics in Office Practice*, **26**(2): 211–224.

Speers AB, Cabey KA, Soumyanath A, et al. 2021. Effects of *Withania somnifera* (Ashwagandha) on stress and the stress- related neuropsychiatric disorders anxiety, depression, and insomnia. *Current Neuropharmacology*, **19**(9): 1468–1495.

Stockwell SR, Platt G, Barrie SE, et al. 2012. Mechanism-based screen for G1/S checkpoint activators identifies a selective activator of EIF2AK3/PERK signalling. *PLoS One*, **7**(1): e28568.

Szuhany KL, Otto MW. 2020. Assessing BDNF as a mediator of the effects of exercise on depression. *Journal of Psychiatric Research*, **123**: 114–118.

Tan HY, Zou W, Jiang JM, et al. 2015. Disturbance of hippocampal H_2S generation contributes to CUMS-induced depression-like behavior: involvement in endoplasmic reticulum stress of hippocampus. *Acta Biochimica et Biophysica Sinica*, **47**(4): 285–291.

Verfaillie T, Rubio N, Garg AD, et al. 2012. PERK is required at the ER-mitochondrial contact sites to convey apoptosis after ROS-based ER stress. *Cell Death & Differentiation*, **19**(11): 1880–1891.

Wang J, Tian LL, He LM, et al. 2018. Lycium barbarum polysaccharide encapsulated poly lactic-co-glycolic acid nanofibers: cost effective herbal medicine for potential application in peripheral nerve tissue engineering. *Scientific Reports*, **8**(1): 8669.

Wang XC, Zhou Y, Chen HX, et al. 2024. ER stress modulates Kv1.5 channels via PERK branch in HL-1 atrial myocytes: relevance to atrial arrhythmogenesis and the effect of tetramethylpyrazine. *Heliyon*, **10**(18): e37767.

Wu CH, Chen JX, Chen C, et al. 2015. Wnt/β-catenin coupled with HIF-1α/VEGF signaling pathways involved in galangin neurovascular unit protection from focal cerebral ischemia. *Scientific Reports*, **5**: 16151.

Wu JJ, Chen YJ, Dobbs N, et al. 2019. STING-mediated disruption of calcium homeostasis chronically activates ER stress and primes T cell death. *Journal of Experimental Medicine*, **216**(4): 867–883.

Xu L, Yang L, Xu HM, et al. 2024. Lycium barbarum glycopeptide ameliorates motor and visual deficits in autoimmune inflammatory diseases. *Phytomedicine*, **129**: 155610.

Yeung KS, Hernandez M, Mao JJ, et al. 2018. Herbal medicine for depression and anxiety: a systematic review with assessment of potential psycho-oncologic relevance. *Phytotherapy Research*, **32**(5): 865–891.

Zhao H, Alexeev A, Chang E, et al. 2005. *Lycium barbarum* glycoconjugates: effect on human skin and cultured dermal fibroblasts. *Phytomedicine*, **12**(1-2): 131–137.

Zimath PL, Dalmagro AP, Mota Da Silva L, et al. 2021. Myrsinoic acid B from *Myrsine coriacea* reverses depressive-like behavior and brain oxidative stress in streptozotocin-diabetic rats. *Chemico-Biological Interactions*, **347**: 109603.